PHYSICAL REVIEW D **86,** 095014 (2012)

Asymmetry at LHC for an $U(1)'$ anomalous extension of MSSM

Francesco Fucito,[1,*] Andrea Mammarella,[1,†] and Daniel Ricci Pacifici[1,‡]

[1]*Dipartimento di Fisica dell'Universit'a di Roma, "Tor Vergata" and I.N.F.N.-Sezione di Roma "Tor Vergata," Via della Ricerca Scientifica, 1-00133 Roma, Italy*

(Received 11 July 2012; revised manuscript received 28 September 2012; published 13 November 2012)

The measurement of the forward-backward asymmetry at LHC could be an important instrument to pinpoint the features of extra neutral gauge particles obtained by an extension of the gauge symmetry group of the standard model. For definitiveness, in this work, we consider an extension of the gauge group of the minimal supersymmetric standard model by an extra anomalous U(1) gauge symmetry. We focus on $pp \to e^+e^-$ at LHC and use four different definitions of the asymmetry obtained implementing four different cuts on the directions and momenta of the final states of our process of interest. The calculations are performed without imposing constraints on the charges of the extra Z's of our model, since the anomaly is cancelled by a Green-Schwarz type mechanism. Our final result is a fit of our data with a polynomial in the charges of the extra U(1) that is used to extract the values of the charges, given the experimental result.

DOI: 10.1103/PhysRevD.86.095014 PACS numbers: 12.60.−i, 14.70.Pw

I. INTRODUCTION

One of the most motivated extensions, from a theoretical point of view, of the standard model (SM) and minimal supersymmetric standard model (MSSM) of particle physics is obtained by enlarging the gauge group of the theory by admitting extra $U(1)$'s. Such extensions are natural at low energy for models coming from grand unified theories and string theories (see Ref. [1] for a recent review). In the string inspired scenarios the anomalies of the extra $U(1)$'s are cancelled by the Green-Schwarz mechanism. To explore such a possibility we will use an extension of the MSSM that from now on will be dubbed MiAUMSSM. An alternative version of this model that admits spontaneous supersymmetry breaking was also formulated in Ref. [2], but in this work we will use the original formulation of Ref. [3]. The phenomenology of the MiAUMSSM has been investigated in different directions. Assuming that the lightest supersymmetric particle (LSP), a candidate for dark matter, comes from the anomalous sector of the model [4,5], the relic density of such LSP was computed and proved to be compatible with the experimental data of WMAP [6]. Furthermore in Ref. [7], the decays of the next to lightest supersymmetric particle into the LSP has been considered, while in Ref. [8] the features of a possible signature of the model at LHC has been considered by concentrating on a particular radiative decay of the next to lightest supersymmetric particle.

In this paper, we will further develop the phenomenology of the MiAUMSSM by computing the forward-backward asymmetry that is induced in the final states of the process $pp \to e^+e^-$ by keeping in account the new gauge boson, Z', associated with the extra $U(1)$ gauge symmetry. The couplings (charges) of this particle to the others present in our model are not fixed by the requirement of gauge anomaly cancellation and can be determined only by experiment. Our aim is to show that such measurement is feasible and that it can be distinguished among the different possible scenarios [9]. Since at the LHC the colliding beams are made of the same particle, to generate an asymmetry in the final state, some cuts on the parameter space have to be necessarily performed. Each possible cut leads to a different definition of the asymmetry. In this work we will use four different sets of cuts to show that our results are not dependent from these choices.

This work is organized as follows: In Sec. II, we briefly review the main features of the model that we are going to study. In Sec. III, we will discuss the four different definitions of the asymmetry we will use; in Sec. IV, we will describe our calculations and collect the results that are finally discussed in the conclusions.

II. MODEL DEFINITION

Our model [3] is an extension of the MSSM with an extra $U(1)$. The charges of the matter fields with respect to the symmetry groups are given in Table I.

The gauge invariance of the model implies

$$\begin{aligned} Q_{U^c} &= -Q_Q - Q_{H_u}, & Q_{D^c} &= -Q_Q + Q_{H_u}, \\ Q_{E^c} &= -Q_L + Q_{H_u}, & Q_{H_d} &= -Q_{H_u}. \end{aligned} \tag{1}$$

Thus, there are only three free charges introduced by the extra symmetry: we can choose Q_Q, Q_L, and Q_{H_u} without loosing generality. The anomalies induced by this extension are cancelled by the Green-Schwarz mechanism; there are no further constraints on the charges.

To evaluate the asymmetry associated with the full process $pp \to e^+e^-$ we have performed the calculation

*Francesco.Fucito@roma2.infn.it
†Andrea.Mammarella@roma2.infn.it
‡Daniel.Ricci.Pacifici@roma2.infn.it

TABLE I. Charge assignment.

	$SU(3)_c$	$SU(2)_L$	$U(1)_Y$	$U(1)'$
Q_i	3	2	1/6	Q_Q
U_i^c	$\bar{3}$	1	−2/3	Q_{U^c}
D_i^c	$\bar{3}$	1	1/3	Q_{D^c}
L_i	1	2	−1/2	Q_L
E_i^c	1	1	1	Q_{E^c}
H_u	1	2	1/2	Q_{H_u}
H_d	1	2	−1/2	Q_{H_d}

of the cross section of the subprocess $q\bar{q} \to e^+e^-$, which we report in Appendix A. In Appendix B we give details on the convolution of this differential cross section for the specific definitions of asymmetry that we will adopt. We take the mass of our Z' to be 1.5 Tev. There are two main reasons for this choice: On the one hand we wanted a sizeble Z' production (see Ref. [3], where there are results for a Z' mass of 1 TeV). On the other hand this mass value allows a comparison with the results in literature [10]. Regardless, our analysis could be repeated for arbitrary value of the Z' mass.

III. ASYMMETRY DEFINITION

Because the initial pp state is symmetric, the asymmetry at the LHC is zero if we integrate over the whole parameter space. However the partonic subprocess $q\bar{q} \to e^+e^-$ is asymmetric. We can keep this asymmetry by imposing kinematical cuts, which are anyway inevitable because of the limits imposed by the detector. There are many possibilities to perform these cuts and each of them leads to a different definition of the asymmetry. In this work we have used the four definitions of the asymmetry, $A_{\mathrm{RFB}}(Y^{\mathrm{cut}})$, $A_{\mathrm{OFB}}(p_z^{\mathrm{cut}})$, $A_{\mathrm{C}}(Y_{\mathrm{C}})$, and $A_{\mathrm{E}}(Y_{\mathrm{C}})$, which are collected in [10]:

$$A_{\mathrm{RFB}} = \left.\frac{\sigma(|Y_{e^-}| > |Y_{e^+}|) - \sigma(|Y_{e^-}| < |Y_{e^+}|)}{\sigma(|Y_{e^-}| > |Y_{e^+}|) + \sigma(|Y_{e^-}| < |Y_{e^+}|)}\right|_{|Y|>Y^{\mathrm{cut}}}, \tag{2}$$

$$A_{\mathrm{OFB}} = \left.\frac{\sigma(|Y_{e^-}| > |Y_{e^+}|) - \sigma(|Y_{e^-}| < |Y_{e^+}|)}{\sigma(|Y_{e^-}| > |Y_{e^+}|) + \sigma(|Y_{e^-}| < |Y_{e^+}|)}\right|_{|p_z|>p_z^{\mathrm{cut}}}, \tag{3}$$

$$A_{\mathrm{C}} = \frac{\sigma_{e^-}(|Y_{e^-}| < Y_{\mathrm{C}}) - \sigma_{e^+}(|Y_{e^+}| < Y_{\mathrm{C}})}{\sigma_{e^-}(|Y_{e^-}| < Y_{\mathrm{C}}) + \sigma_{e^+}(|Y_{e^+}| < Y_{\mathrm{C}})}, \tag{4}$$

$$A_{\mathrm{E}} = \frac{\sigma_{e^-}(Y_{\mathrm{C}} < |Y_{e^-}|) - \sigma_{e^+}(Y_{\mathrm{C}} < |Y_{e^+}|)}{\sigma_{e^-}(Y_{\mathrm{C}} < |Y_{e^-}|) + \sigma_{e^+}(Y_{\mathrm{C}} < |Y_{e^+}|)}, \tag{5}$$

where σ is the total cross section after integrating with the partonic distribution functions (PDFs).

The first two asymmetries are defined in the center of mass (CM) frame. The forward-backward asymmetry A_{RFB} [1,9,11–14] has a cut on the rapidity Y of the e^-/e^+ pair

$$Y = \frac{1}{2}\log\left(\frac{E_{e^-e^+} + p_z}{E_{e^-e^+} - p_z}\right). \tag{6}$$

The one-side asymmetry A_O [15,16] has a cut on p_z, the total momentum associated with the final states (e^-e^+) moving longitudinally along the beam direction chosen to be the z axis.

In Appendix B this rapidity will be expressed in the CM in terms of the partonic variables $x_{1,2}$. $E_{e^-e^+}$ is the sum of the energies associated with the two particles. The other two asymmetries are defined in the laboratory (Lab) frame. The variable $Y_{e^\pm}$ is the pseudorapidity associated with the single particle $e^\pm$ and expressed as

$$Y_{e^\pm} = -\log(\tan(\theta^{e^\pm}/2)), \tag{7}$$

with $\theta^{e^\pm}$ the angle of the outgoing fermion with respect to the z axis. In this case the kinematical cut is over the rapidity in the Lab frame that is denoted by Y_C and that will be introduced in Appendix B. The central asymmetry A_C [17–21] is calculated integrating in the angular region centered on the axis orthogonal to the beam, while the edge asymmetry A_E [22] is defined in the complementary region.

For further details, see Appendix B.

IV. ASYMMETRY CALCULATION

In this work we have calculated the asymmetry in two different ways. First we have used a numerical code that we have written using Mathematica. This code uses the cross section calculated in Appendix A to numerically compute the integrals discussed in Appendix B. As a second check we have repeated the same computation using the HERWIG package [23,24], that we have modified to calculate the asymmetry. We have chosen to repeat twice our computation for two main reasons: the first one is that in this way we can have a cross check between our results; the second is that these methods have different peculiarities that we want to use. For example, the numerical integration is less computer time consuming for the Mathematica code, which helps in establishing the dependence of the asymmetry from the free charges of the model. At the same time the HERWIG package permits one to study how the cuts influence the rate of production of our final state. For these reasons we have performed the basic calculation (i.e., the asymmetry optimization) using both methods. We remark that all the results that we will show are strongly dependent on the set of PDFs used to calculate them and that this leads to a systematical error. In the following we do not show results for different sets of PDFs. Where the statistical error is concerned, we have estimated it using the formula [10]

$$\mathrm{err} \equiv \sqrt{\frac{4N_F N_B}{N^3}} \simeq \frac{1}{\sqrt{\mathcal{L}\sigma}}, \tag{8}$$

where $N_{F/B}$ are the forward/backward events, N is the total number of events, and $\mathcal{L}$ is the luminosity. In the following we show the estimated errors for the asymmetry definitions keeping $\mathcal{L} = 100\ \text{fb}^{-1}$.

We aim to use the asymmetry to distinguish our model from the MSSM or other models that include an extra $U(1)$. In the following we will perform the asymmetry calculation around the peak region, that is for $M_{Z'} - 3\Gamma_{Z'} < M_{e^+e^-} < M_{Z'} + 3\Gamma_{Z'}$, where $\Gamma_{Z'}$ is the total decay rate of the Z'. As we remarked in Appendix B, this determines the integration domain, that is $(M_{Z'} - 3\Gamma_{Z'})^2 < s < (M_{Z'} + 3\Gamma_{Z'})^2$. We also compare our results with the ones obtained for the sequential standard model (SSM), in which there is an extra Z' boson that has the same couplings to fermions such as the SM Z boson [1,25]. See Sec. IV D for further details on the corresponding Lagrangian and the values of the quantum numbers.

A. Optimized asymmetry

As shown in Ref. [10] the asymmetry magnitude is not a good function to optimize. A better choice is, instead, the statistical significance:

$$\text{Sig} \equiv A\sqrt{\mathcal{L}\sigma}, \tag{9}$$

where A can be any of the previously defined asymmetries, $\mathcal{L}$ is the LHC integrated luminosity, which we take to be $100\ \text{fb}^{-1}$.

We have found a good agreement between the results obtained by using the Mathematica code and those obtained with the event simulator HERWIG. Thus, we are confident that our results will be reliable to calculate other observables, e.g., the dependence from the charges of the asymmetries and the significancies. In Fig. 1, we show the results for the on-peak significance of the MiAUMSSM and SSM for all the definitions of asymmetry that we use. The best cuts are those that maximize the significance. For the SSM we find the same values as in Ref. [10]. We list the best cuts of the MiAUMSSM in Table II. As in Ref. [10], we expect that the best cuts are nearly independent from the charges and depend only on the Z' mass and the partonic distribution functions. Moreover they are also essentially independent from the specific model chosen as it is confirmed by our analysis. As a further check we have performed simulations with the SSM. We have used the same settings of Ref. [10], obtaining very similar results for all the cuts, confirming the reliability of our numerical codes. We used the SSM not only for having a check of the validity of our calculations but also to have results that can be compared with those of the MiAUMSSM.

B. Dependence on the charges

Now we want to use the best cuts previously found to study the asymmetry in function of the free charges of our

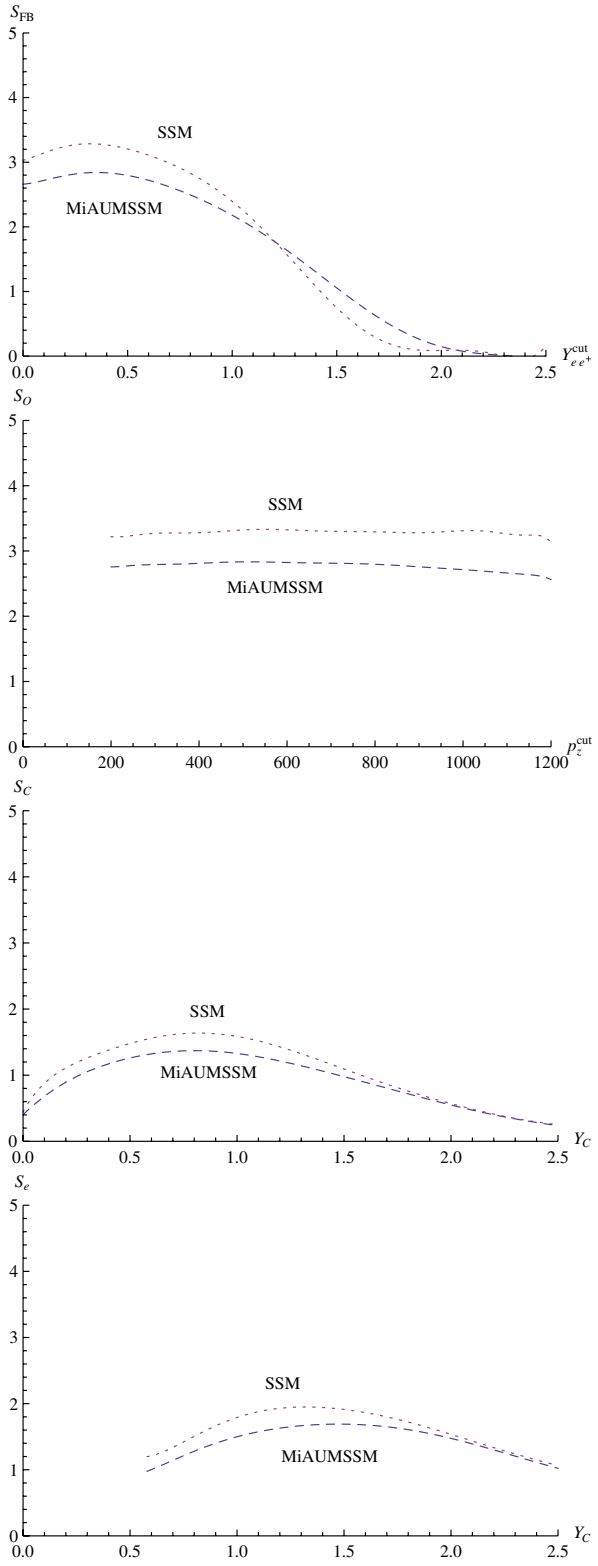

FIG. 1 (color online). Significance as a function of the corresponding cut associated with the four definitions of asymmetry for on-peak events in both the MiAUMSSM and the SSM (calculated with the HERWIG package). The charges have been fixed: $Q_{H_u} = 0.5$, $Q_Q = 0.75$ and $Q_L = 1$. The shape of these functions depends on this choice while the position of the peak does not.

TABLE II. Best cuts for the on-peak e^+e^- asymmetries.

	A_{RFB}	A_O	A_C	A_E
Best cut	$Y^{\mathrm{cut}}_{f\bar{f}} = 0.4$	$p^{\mathrm{cut}}_{z,f\bar{f}} = 580$ GeV	$Y_C = 0.8$	$Y_C = 1.4$

model. We have studied the value of the four asymmetries keeping alternatively one of the charges fixed to 0 and varying the other two from -1 to 1. We choose these ranges because in the SM all the charges are of this order. Furthermore in Ref. [5], we have found that $-1 \lesssim Q_{H_u} \lesssim 1$ for the model to be consistent with the WMAP data on dark matter. Then, out of simplicity we have used the same region for the other two charges. As was mentioned, we have obtained the following plots using Mathematica to perform the numerical integration. Some of the results we have obtained are shown in Figs. 2–4. The contour plots for the other cases can be found in Ref. [26].

In these plots the darkest color areas are those with the lowest absolute values of the asymmetry while the greatest values lie in the lightest color region. In addition, these plots are almost symmetric under exchanges in the signs of the charges. The contour plots with $Q_{H_u} = 0$ are almost invariant under the exchange $Q_i \to -Q_i$ of the two remaining charges. Those with $Q_L = 0$ or $Q_Q = 0$ are almost symmetric only under the change of sign of both the two unfixed charges. So the asymmetry as a function of the charges must reflect these sorts of symmetries in its polynomial dependence on the charges. This implies that if we try to fit the asymmetry with a rational function [which is the best choice, given the definitions (2)–(5)] we will have constraints on the coefficients of the fit.

C. Number of events

We already mentioned that to obtain a nonzero asymmetry at LHC we have to impose cuts in the parameter space. Obviously these cuts will diminish the number of events that we can use to measure the asymmetry. It is important to be sure that they do not drastically affect the set of data we have at our disposal. To study the ratio between the number of events obtained applying the cuts and the total number of events expected in our channel of interest ($pp \to e^+e^-$), we have used the HERWIG package. We have studied the ratio N_i/N_{tot_i}, where N_i is the sum of the forward and backward events for the ith definition of asymmetry and N_{tot_i} is the number of events that we have generated with HERWIG. We have performed the calculation of N_i/N_{tot_i} in two cases:

(i) on peak invariant mass, variable cuts;
(ii) variable invariant mass, fixed cuts.

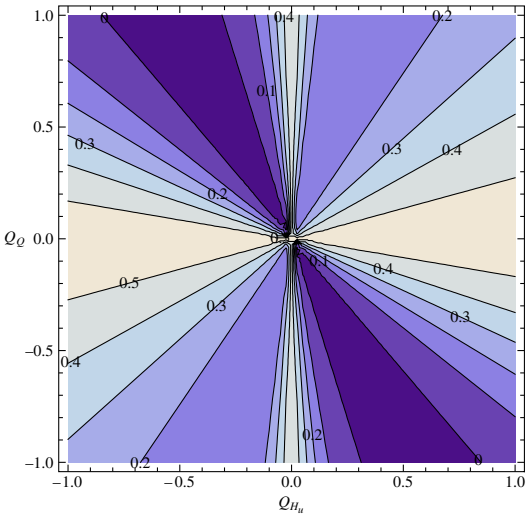

FIG. 2 (color online). Results for the forward-backward asymmetry with $Q_L = 0$ for the best cuts.

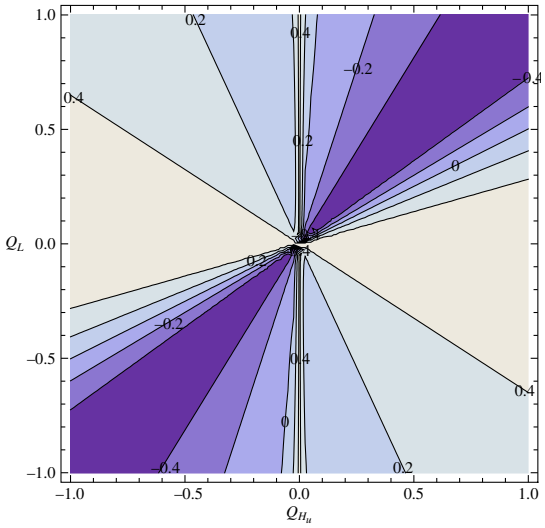

FIG. 3 (color online). Results for the forward-backward asymmetry with $Q_Q = 0$ for the best cuts.

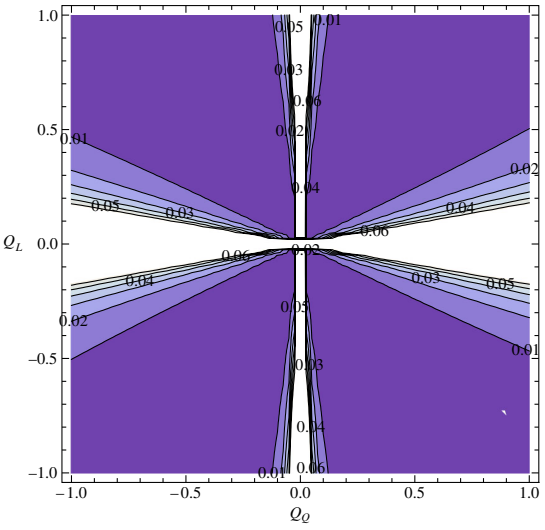

FIG. 4 (color online). Results for the forward-backward asymmetry with $Q_{H_u} = 0$ for the best cuts.

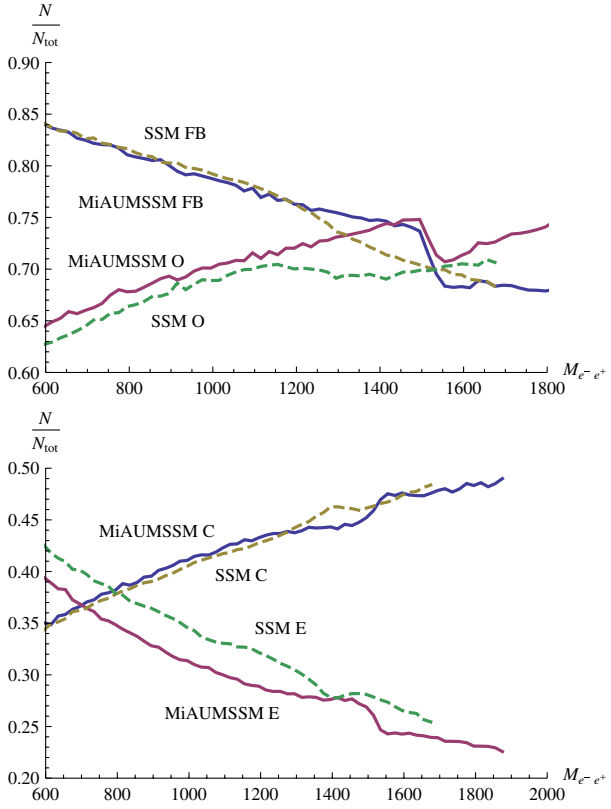

FIG. 5 (color online). N_i/N_{tot_i} as a function of the invariant mass, with the cuts kept fixed, for the four definitions of asymmetry. In the upper (lower) figure we display the results for the FB and O (C and E) asymmetries for the MiAUMSSM (thick lines) and the SSM (dashed lines).

Only in the case of a variable invariant mass with a fixed cut is it possible to distinguish the behavior of our model from that of the SSM. Therefore we show only the related results in Fig. 5. After the implementation of the cuts we are left with 65%–75% of the total number of events for the FB and O asymmetry, while for the C and E asymmetries we are left with 40%–50% of the events. In both cases these ratios are good enough to allow the measurement of the observable of interest.

D. Comparison with other models: LRM and SSM

In this subsection, we present a brief analysis of the results for the asymmetry obtained with two well-known models of extra $U(1)$ extension of the SM: the left-right model (LRM) [11,13] and the previously mentioned SSM [25]. We will see that the asymmetry in our anomalous model almost always leads to values that can be distinguished from those of the LRM and SSM. This implies that a possible future measure could discriminate among these models. The couplings among the fermions and the Z' for all these models could all be written in the form

$$g_{Z'} J^{\mu}_{Z'} Z'_{\mu} = \alpha \sum_f \bar{\psi}_f \gamma^{\mu} (g_V^f - g_A^f \gamma_5) \psi_f Z'_{\mu}, \tag{10}$$

where

$$\alpha = \begin{cases} -\frac{g}{2\cos\theta_W} & \text{SSM} \\ \frac{e}{2\cos\theta_W} & \text{LRM} \\ g_0 & \text{MiAUMSSM} \end{cases}. \tag{11}$$

The charges g_V^f and g_A^f are given explicitly in Table III. θ_W is the Weinberg angle, defined by $\sin^2\theta_W = 0.231$. In the case of the LRM we have chosen the so-called symmetric version, for which $\alpha_{\text{LR}} = 1.59$ [11,13]. Using HERWIG, we have calculated the on-peak asymmetry for these two models. Obviously in the case of the MiAUMSSM we do not have a unique value for the asymmetry, because in the model the charges are not fixed. To show that it is possible to distinguish the MiAUMSSM from the other models, we have to estimate the statistical error in this measurement, by using the formula (8). The exact values depend on the cross section that is model dependent. Now, if we fix $Q_{H_u} = Q_Q = Q_L = 0.5$, the resulting values for the asymmetries associated with the three models are shown in Fig. 6. The data plotted in the figure show that it is always possible to discriminate the anomalous model from the nonanomalous ones.

Now we want to stress that the three charges of our model are free but the couplings of the fermions to the Z' in the anomalous MiAUMSSM have a peculiar functional form given in Table III. As a consequence, it is not possible to match the couplings to the extra Z' of the MiAUMSSM with those of other models. But, since the four asymmetries have associated statistical errors, we could have a range of values of our three charges where the couplings of the MiAUMSSM (and consequently the asymmetries) could be matched with those of the SSM and LRM models within the considered errors. In reality this does not happen as we

TABLE III. Couplings of the SM fermions to the Z's for the SSM, LRM, and MiAUMSSM models.

	SSM		LRM		MiAUMSSM	
f	g_V^f	g_A^f	g_V^f	g_A^f	g_V	g_A
e, μ, τ	$-\frac{1}{2} + 2\sin^2\theta_W$	$-\frac{1}{2}$	$\frac{1}{\alpha_{\text{LR}}} - \frac{\alpha_{\text{LR}}}{2}$	$\frac{\alpha_{\text{LR}}}{2}$	$Q_L - Q_{H_u}/2$	$Q_{H_u}/2$
u, c, t	$\frac{1}{2} - \frac{4}{3}\sin^2\theta_W$	$\frac{1}{2}$	$-\frac{1}{3\alpha_{\text{LR}}} + \frac{\alpha_{\text{LR}}}{2}$	$-\frac{\alpha_{\text{LR}}}{2}$	$Q_Q + Q_{H_u}/2$	$-Q_{H_u}/2$
d, s, b	$-\frac{1}{2} + \frac{2}{3}\sin^2\theta_W$	$-\frac{1}{2}$	$-\frac{1}{3\alpha_{\text{LR}}} - \frac{\alpha_{\text{LR}}}{2}$	$\frac{\alpha_{\text{LR}}}{2}$	$Q_Q - Q_{H_u}/2$	$Q_{H_u}/2$

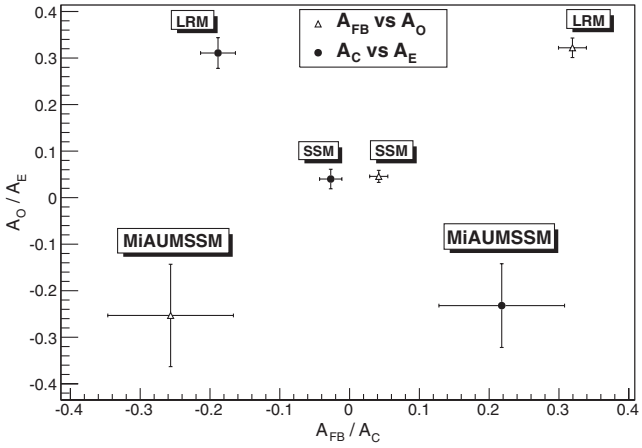

FIG. 6. The bullets (triangles) define the $A_{\rm FB}$ and A_O (A_C and A_E) for the three models considered in the main text. The charges of the MiAUMSSM are all fixed to 0.5.

can infer from Fig. 7, where we consider an error up to 25%, much bigger than the expected experimental error. Observing the amount of points in these figures, it is evident that the SSM is closer to our model than the LRM. This is the reason why throughout this paper we focus our analysis on the comparison with the SSM.

E. General case

In this section, we want to find the function that describes the asymmetry in terms of the three free charges of our model that can assume values between -1 and 1. From the cross section of the process, that can be found in Appendix A, we can see that the amplitude is proportional to the fourth power of the charges. Thus, Eqs. (2)–(5), imply that the asymmetry must be a rational function in which both the numerator and denominator are fourth grade polynomials in the charges:

$$A = \frac{\sum_{i,j,k=0}^{n} a_{ijk} (Q_{H_u})^i (Q_Q)^j (Q_L)^k}{\sum_{i,j,k=0}^{n} b_{ijk} (Q_{H_u})^i (Q_Q)^j (Q_L)^k}, \tag{12}$$

with $i + j + k = n \leq 4$.

The apparent symmetries of the contour plots obtained in Sec. IV B imply that the terms of odd degree in the charges are suppressed. Then the only relevant terms that do not contain Q_{H_u} are Q_Q^2, Q_L^2, Q_Q^4, Q_L^4, and $Q_Q^2 Q_L^2$, while for the terms that do not contain Q_Q or Q_L we can also have terms of the form $Q_i^3 Q_j$ or $Q_i Q_j$ where i, j are the two free charges of each case. For example, a term proportional to $Q_Q^3 Q_L$ is suppressed, while a term proportional to $Q_Q^3 Q_{H_u}$ is present. Fitting our data for the on-peak asymmetries with the functional form (12), we find the coefficients a_{ijk}'s of (12). Then considering only three of the four definitions, we obtain a nonlinear system with three equations and three variables (Q_{H_u}, Q_Q, and Q_L) that could be solved numerically. In this way the asymmetry is useful for fixing the values of the $U(1)'$ charges. Moreover, once the values of the three charges are obtained by the previous system; the fourth definition of asymmetry can be used as a check for the validity of the model under scrutiny. In fact, its hypothetical experimental value must be recovered by using (12) with the values of the charges already found, within the considered error (we use the mean relative error for each asymmetry definition). In the Appendix C we write a table with the coefficients of the four fits. As expected, we have found out that the odd degree polynomials have negligible coefficients, thus confirming the intuitions stemming from the analysis of the contour plots. The exactness of the fit is evaluated computing the R^2 (called coefficient of determination; a perfect fit has $R^2 = 1$) and the medium relative error for these results. The results are shown in Table IV, attesting the accuracy of the procedure. In particular, the R^2 value states (as we expected) that the errors in our fits are almost

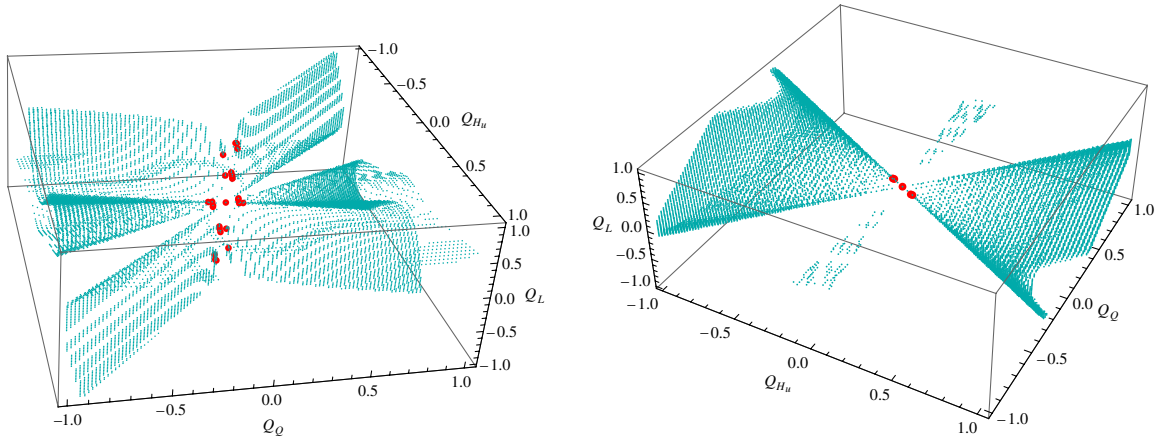

FIG. 7 (color online). Values of the charges that give a MiAUMSSM asymmetry close to the SSM asymmetry within errors of 15 (big red dots), 25% (left) and to the LRM within errors of 20 (big red dots), 25% (right).

TABLE IV. R^2 and medium relative error for the polynomial fit of the asymmetry with respect to the three charges.

	A_{RFB}	A_O	A_C	A_E
R^2	0,999	0,999	0,999	0,999
MRE	0.008	0.009	0.019	0.017

completely due to the numerical approximations in the calculation of the integrals and due to the uncertainties of the PDFs.

V. CONCLUSION

We have numerically calculated the LHC asymmetry of the MiAUMSSM using four different definitions, namely, forward-backward, one-side, central, and edge asymmetries for the process $pp \to e^+e^-$. An analogous study with a complete simulation of the ATLAS detector has been carried out for the SM asymmetry [27]. The performance of the detector will be unaltered for a measurement in the TeV range (where there are hopes of finding the Z') meaning that our results should be robust even in the case of a complete analysis in which there is a full simulation of the detector. In this respect, the good agreement, shown in Table 6.4 of [28], for the results coming from PYTHIA versus those coming from the real measurement testifies the good degree of precision of the Monte Carlo simulators for these kinds of computations. In our case, to achieve a statistics comparable to that collected for the case studied in Ref. [27], at least 100 fb^{-1} will be needed, and this will be achieved most likely in 2015 when the machine will work at $\sqrt{s} = 14$–15 TeV after the planned shutdown in 2013/2014.

To infer the optimal cuts to use, we have maximized the significance related to each asymmetry. We have verified, as it is expected from Ref. [10], that these cuts are nearly independent from the free charges of our model. Then we have used these optimal cuts to investigate the asymmetry behavior in function of pairs of free charges, keeping the third fixed to 0 to have a graphical representation of the results. Furthermore, we have found that the asymmetry is invariant under $Q_i \to -Q_i$. We have checked that even in the presence of the cuts needed to evaluate the asymmetry, the number of leftover events is such to lead to a meaningful measurement.

We have further shown that the MiAUMSSM is distinguishable from the SSM and LRM models, showing examples of different predictions for the asymmetries that differ at least for a good 20% of their value. Finally, we have studied the four asymmetries as functions of the three charges and have fitted the results as a rational function of polynomials of degree four in the charges. The fit is found to be accurate, with a $R^2 = 0.999$ for all the definitions we have used.

ACKNOWLEDGMENTS

The authors would like to thank G. Cattani, G. Corcella, A. Lionetto, B. Panico, A. Racioppi, B. Xiao, and Y.-k. Wang for useful discussions and correspondence during the completion of this paper.

APPENDIX A: CROSS SECTION

We have calculated the cross section in the CM for the process $q\bar{q} \to e^+e^-$ for a general Drell-Yan interaction in which we can have the product of diagrams where the γ, Z_0, and Z' can be exchanged. Thus we have six possible terms: $\gamma\gamma$, γZ_0, $\gamma Z'$, Z_0Z_0, Z_0Z', and $Z'Z'$.

The total amplitude is

$$|M|^2(q) = \frac{1}{3}\frac{1}{4}\sum_{a,b=\gamma,Z,Z'} g_a^2 g_b^2 M_{ab}, \tag{A1}$$

where the fractions $\frac{1}{4}$ and $\frac{1}{3}$ come out from the averages over spin and color, and g_0 is the coupling associated with the Z'. We fix its value to 0.1. M_{ab} is the amplitude of each process divided by the couplings:

$$\begin{aligned} M_{ab} = {} & \frac{64N_{ab}[(s-m_a^2)(s-m_b^2)+(\Gamma_a m_a \Gamma_b m_b)]}{[(s-m_a^2)^2+(\Gamma_a m_a)^2][(s-m_b^2)^2+(\Gamma_b m_b)^2]}\{2m_e^2 m_q^2 \mathcal{C}_{e,-}^{AAVV}\mathcal{C}_{q,-}^{AAVV} - m_e^2(p_q\cdot p_{\bar{q}})\mathcal{C}_{e,-}^{AAVV}\mathcal{C}_{q,+}^{AAVV} \\ & + [(p_q\cdot p_{\bar{e}})(p_{\bar{q}}\cdot p_e) - (p_q\cdot p_e)(p_{\bar{q}}\cdot p_{\bar{e}})]\mathcal{C}_{e,+}^{VAAV}\mathcal{C}_{q,+}^{VAAV} + +[(p_q\cdot p_{\bar{e}})(p_{\bar{q}}\cdot p_e) \\ & + (p_q\cdot p_e)(p_{\bar{q}}\cdot p_{\bar{e}})]\mathcal{C}_{e,+}^{AAVV}\mathcal{C}_{q,+}^{AAVV} + -m_q^2(p_e\cdot p_{\bar{e}})\mathcal{C}_{e,+}^{AAVV}\mathcal{C}_{q,-}^{AAVV}\} \end{aligned} \tag{A2}$$

defining $\mathcal{C}_{i,\pm}^{MNPQ} = C_{i,a}^M C_{i,b}^N \pm C_{i,a}^P C_{i,b}^Q$, with $i = e$, q and $M, N, P, Q = V, A$. In this expression N_{ab} is a multiplicity factor that is equal to $\frac{1}{2}$ if the exchanged vector bosons are identical and is equal to 1 if they are different. The C's are simply the vector and axial quantum numbers related to the vector bosons: for the γ and the Z_0 they are the usual SM quantum numbers that can be found in Ref. [29], while the vector and axial couplings related to the Z' have been calculated in Ref. [26] and are shown in Table V.

We remark that in this cross section there are only terms of degree four in the powers of the charges. However, from Eq. (A1) we know that there are different contributions to the total squared amplitude of our process. These terms are

TABLE V. Vector and axial quantum numbers of the SM fermions with respect to Z'.

	$C^V_{f,Z'}$	$C^A_{f,Z'}$
$f = u, c, t$	$Q_Q + Q_{H_u}/2$	$-Q_{H_u}/2$
$f = d, s, b$	$Q_Q - Q_{H_u}/2$	$Q_{H_u}/2$
$f = e, \mu, \tau$	$Q_L - Q_{H_u}/2$	$Q_{H_u}/2$

divided into three types: the term $Z'Z'$; the terms $\gamma Z'$ and $Z_0 Z'$; and those $\gamma\gamma$, γZ_0, and $Z_0 Z_0$ that give contributions of degree four, two, and zero in the anomalous charge, respectively. Since we are studying the on-peak region, we expect the contribution from the $Z'Z'$ channel to be dominant with respect to the others: this is evident from the table of the coefficients shown in Appendix C. Observing the previous formula, we can see that all the combinations of C's contain two C_q and two C_e because our elementary process involves two leptons and two quarks. Observing that Q_Q and Q_L are related to C_q and C_e, respectively, this implies that we cannot have terms of degree larger than 2 in Q_Q and Q_L. This is verified by our fit, where the coefficients related to this terms are suppressed (see Appendix C). The differential cross section can be found multiplying for the usual kinematic prefactor and summing this result over the contribution of the six possible initial quarks:

$$\left.\frac{\partial^2\sigma}{\partial s\,\partial\cos\theta}\right|_{\rm CM} = \sum_q \frac{p_e}{32\pi s p_q}|M|^2(q). \tag{A3}$$

APPENDIX B: DETAILS ON THE ASYMMETRY DEFINITIONS

The explicit expression of Eq. (2) in the CM frame is

$$A_{\rm RFB} = \frac{\int_{C_{\rm cut}} dx_1 dx_2 \sum_q f_q(x_1) f_{\bar q}(x_2)(F - B)}{\int_{C_{\rm cut}} dx_1 dx_2 \sum_q f_q(x_1) f_{\bar q}(x_2)(F + B)}, \tag{B1}$$

where

$$F = \int_0^1 d\cos\theta \frac{d\sigma(\cos\theta, s)}{d\cos\theta ds}, \qquad B = \int_{-1}^0 d\cos\theta \frac{d\sigma(\cos\theta, s)}{d\cos\theta ds} \tag{B2}$$

are the forward and backward contributions, respectively.

The $f_{q/\bar q}(x_i)$ are the PDFs of $q/\bar q$. $C_{\rm cut}$ is the domain of integration, which depends on the type of asymmetry that we want to calculate according to the definitions (2)–(5).

The couples of variables (x_1, x_2) and (s, Y) are not independent. In fact, their definition is $s = S x_1 x_2$ and $Y = \frac{1}{2}\log(x_1/x_2)$, where $S = (14\ \text{TeV})^2$ is the total squared energy of the accelerator.

Since we have calculated the cross section of the process (see Appendix A) that we are going to study with respect to s, we perform the change of variables $(x_1, x_2) \to (s, Y)$ in the expression (B1). The Jacobian of this transformation is $J = 1/S$. Now we focus on the integral $\int_{-\infty}^{-Y_{\rm cut}} dY$: if we perform the change of variable $Y \to -Y$, because of the Y definition, this corresponds to the exchange $x_1 \leftrightarrow x_2$ and consequently to the exchange of forward with backward $(F \leftrightarrow B)$. Summarizing,

$$\int_{-\infty}^{-Y_{\rm cut}} dY \sum_q f_q(x_1) f_{\bar q}(x_2)(F \pm B) = \int_{Y_{\rm cut}}^{\infty} dY \sum_q f_q(x_2) f_{\bar q}(x_1)(\pm F + B). \tag{B3}$$

Using this result we obtain the formula that we implemented in the Mathematica evaluation, that is

$$A_{\rm RFB} = \frac{\int ds J \int_{Y_{\rm cut}}^{+\infty} dY \sum_q f^-_{q\bar q}(x_1(s,Y), x_2(s,Y))(F - B)}{\int ds J \int_{Y_{\rm cut}}^{+\infty} dY \sum_q f^+_{q\bar q}(x_1(s,Y), x_2(s,Y))(F + B)}, \tag{B4}$$

with

$$f^{\pm}_{q\bar q}(x_1, x_2) = f_q(x_1) f_{\bar q}(x_2) \pm f_{\bar q}(x_1) f_q(x_2). \tag{B5}$$

The formula for A_O is very similar and it is obtained by replacing Y with p_z. This leads to a different cut and a different Jacobian.

The expressions for A_C and A_E are also very similar between them and we present them together. In these two cases the cut is performed on the angle $\theta^{\rm cut}$ and therefore on the limits of integration for F and B. These asymmetries are defined in the Lab frame, because the Lorentz transformation from the CM frame "squeezes" the final particles [17]. The angles of the outgoing $e^{\mp}$ with respect to the z axis, denoted by $\pm\theta$, respectively, in the CM frame, are replaced by θ^{e^-} and θ^{e^+} in the Lab frame where the outgoing $e^{\pm}$ no longer have the same direction. Therefore, in the Lab frame, instead of the definitions (B2), we have

$$\begin{aligned}(F/B)_C &= \int_{-\rm cut}^{+\rm cut} \frac{d\sigma}{d\cos\theta^{e^{(-/+)}} ds} d\cos\theta^{e^{(-/+)}} \\ (F/B)_E &= \int_{-1}^{-\rm cut} \frac{d\sigma}{d\cos\theta^{e^{(-/+)}} ds} d\cos\theta^{e^{(-/+)}} \\ &\quad + \int_{\rm cut}^{+1} \frac{d\sigma}{d\cos\theta^{e^{(-/+)}} ds} d\cos\theta^{e^{(-/+)}},\end{aligned} \tag{B6}$$

where the limit of integration *cut* is defined in terms of $\theta^{\rm cut}$ as $\text{cut} = \cos\theta^{\rm cut}$. Then (4) and (5) become

$$A_{C/E} = \int ds \int_{s/S}^1 dx_1 J \sum_q f_q(x_1) f_{\bar q}(x_2)(F_{C/E} - B_{C/E}), \tag{B7}$$

where $x_2 = \frac{s}{S x_1}$. J is now the Jacobian of the transformation $(x_1, x_2) \to (x_1, s)$.

The cut parameter that enters in the definitions (4) and (5) is not directly $\theta^{\rm cut}$ but the associated pseudorapidity $Y_C = -\log(\tan(\theta^{\rm cut}/2))$. For further details on the calculations sketched in this Appendix, see Ref. [26].

APPENDIX C: COEFFICIENTS OF THE POLYNOMIAL FIT

We have performed a numerical calculation of the asymmetries letting the three charges vary in the $-1 < Q_i < 1$ range. Then we have fitted the results with the rational function (12). We have found that only the even grade terms contribute to the results, so we neglect the odd grade terms.

Another point to note is that the formula (12) implies that all the coefficients a_{ijk} and b_{ijk} are defined up to a global multiplicative factor. To permit the comparison among the different types of asymmetries, we have fixed $a_{400} = 1$ (or $a_{400} = -1$ for the C asymmetry that assumes opposite sign with respect to the others). However, if such type of models will be discovered at the LHC, this value will be fixed differently to match the experimental results. The coefficients' values for our choice are listed in Table VI. Note that this table contains only the statistical error and not the systematic error due to the choice of the PDFs.

TABLE VI. Coefficients of the fits for the four definitions of asymmetry.

	A_{RFB}	A_O	A_C	A_E
a_{000}	$(-0.52 \pm 0.02) \times 10^{-6}$	$(-0.31 \pm 0.04) \times 10^{-6}$	$(1.18 \pm 0.04) \times 10^{-6}$	$(0.86 \pm 0.18) \times 10^{-6}$
a_{200}	$(82 \pm 3) \times 10^{-6}$	$(58 \pm 5) \times 10^{-6}$	$(-17 \pm 5) \times 10^{-6}$	$(140 \pm 21) \times 10^{-6}$
a_{020}	$(9.9 \pm 1.5) \times 10^{-6}$	$(9 \pm 2) \times 10^{-6}$	$(-27 \pm 3) \times 10^{-6}$	$(12 \pm 11) \times 10^{-6}$
a_{002}	$(5.2 \pm 1.4) \times 10^{-6}$	$(2 \pm 2) \times 10^{-6}$	$(11 \pm 2) \times 10^{-6}$	$(61 \pm 10) \times 10^{-6}$
a_{110}	$(5 \pm 3) \times 10^{-6}$	$(4 \pm 5) \times 10^{-6}$	$(19 \pm 6) \times 10^{-6}$	$(113 \pm 24) \times 10^{-6}$
a_{101}	$(-18 \pm 4) \times 10^{-6}$	$(-6 \pm 6) \times 10^{-6}$	$(-148 \pm 7) \times 10^{-6}$	$(-269 \pm 27) \times 10^{-6}$
a_{011}	$(-80 \pm 3) \times 10^{-6}$	$(-65 \pm 5) \times 10^{-6}$	$(34 \pm 5) \times 10^{-6}$	$(-177 \pm 22) \times 10^{-6}$
a_{400}	1(fixed)	1(fixed)	-1(fixed)	1(fixed)
a_{040}	0.015638 ± 0.000004	0.015634 ± 0.000006	-0.015444 ± 0.000007	0.01552 ± 0.00003
a_{004}	0.000969 ± 0.000002	0.000967 ± 0.000004	-0.000984 ± 0.000004	0.000964 ± 0.000018
a_{310}	0.88011 ± 0.00005	0.87460 ± 0.00007	-0.85003 ± 0.00008	0.8573 ± 0.0003
a_{220}	0.01525 ± 0.00004	0.01544 ± 0.00006	-0.01565 ± 0.00007	0.0163 ± 0003
a_{130}	-0.000729 ± 0.000019	-0.00061 ± 0.00003	0.00077 ± 0.00003	-0.00113 ± 0.00013
a_{301}	-1.99340 ± 0.00005	-1.99305 ± 0.00008	1.99360 ± 0.00009	-1.9930 ± 0.0004
a_{211}	-1.75973 ± 0.00010	-1.74845 ± 0.00016	1.69973 ± 0.00018	-1.7141 ± 0.0007
a_{121}	-0.00388 ± 0.00007	-0.00403 ± 0.00011	0.00429 ± 0.00012	-0.0052 ± 0.0005
a_{031}	0.00165 ± 0.00002	0.00128 ± 0.00003	-0.00188 ± 0.00004	0.00244 ± 0.00015
a_{202}	0.00456 ± 0.00010	0.00438 ± 0.00016	-0.00463 ± 0.00018	0.0048 ± 0.0007
a_{112}	-0.00049 ± 0.00009	-0.00044 ± 0.00014	0.00013 ± 0.00015	-0.0011 ± 0.0006
a_{022}	0.00773 ± 0.00003	0.07740 ± 0.00005	-0.00778 ± 0.00006	0.0068 ± 0.0002
a_{103}	-0.001244 ± 0.000013	-0.00120 ± 0.00002	0.00136 ± 0.00002	-0.00170 ± 0.00009
a_{013}	0.000181 ± 0.000015	0.00023 ± 0.00002	-0.00014 ± 0.00003	0.00047 ± 0.00011
b_{000}	$(-1.19 \pm 0.06) \times 10^{-6}$	$(-0.70 \pm 0.09) \times 10^{-6}$	$(-3.19 \pm 0.12) \times 10^{-6}$	$(2.2 \pm 0.4) \times 10^{-6}$
b_{200}	$(121 \pm 7) \times 10^{-6}$	$(181 \pm 12) \times 10^{-6}$	$(-88 \pm 16) \times 10^{-6}$	$(-637 \pm 57) \times 10^{-6}$
b_{020}	$(23 \pm 4) \times 10^{-6}$	$(21 \pm 6) \times 10^{-6}$	$(74 \pm 7) \times 10^{-6}$	$(29 \pm 28) \times 10^{-6}$
b_{002}	$(12 \pm 3) \times 10^{-6}$	$(5 \pm 5) \times 10^{-6}$	$(-29 \pm 6) \times 10^{-6}$	$(154 \pm 25) \times 10^{-6}$
b_{110}	$(-58 \pm 26) \times 10^{-6}$	$(51 \pm 41) \times 10^{-6}$	$(-282 \pm 52) \times 10^{-6}$	$(2392 \pm 204) \times 10^{-6}$
b_{101}	$(-116 \pm 13) \times 10^{-6}$	$(-207 \pm 20) \times 10^{-6}$	$(408 \pm 27) \times 10^{-6}$	$(-392 \pm 100) \times 10^{-6}$
b_{011}	$(85 \pm 39) \times 10^{-6}$	$(-82 \pm 62) \times 10^{-6}$	$(-104 \pm 79) \times 10^{-6}$	$(-1120 \pm 306) \times 10^{-6}$
b_{400}	1.90571 ± 0.00004	1.90585 ± 0.00006	2.28541 ± 0.00008	2.1465 ± 0.0003
b_{040}	0.036021 ± 0.000010	0.036021 ± 0.000016	0.04190 ± 0.00002	0.03945 ± 0.00008
b_{004}	0.002232 ± 0.000006	0.002229 ± 0.000009	0.002670 ± 0.000012	0.00245 ± 0.00005
b_{310}	1.40007 ± 0.00018	1.3899 ± 0.0003	1.3347 ± 0.0004	1.2650 ± 0.0015
b_{220}	3.8269 ± 0.0003	3.8323 ± 0.0004	4.5879 ± 0.0006	4.338 ± 0.002
b_{130}	-0.00386 ± 0.00018	-0.0033 ± 0.0003	-0.0035 ± 0.0004	-0.0103 ± 0.0014
b_{301}	-3.79461 ± 0.00014	-3.7943 ± 0.0002	-4.5504 ± 0.0003	-4.2761 ± 0.0011
b_{211}	-2.7984 ± 0.0004	-2.7775 ± 0.0007	-2.6661 ± 0.0009	-2.533 ± 0.003
b_{121}	-7.5882 ± 0.0007	-7.5998 ± 0.0011	-9.1030 ± 0.0014	-8.592 ± 0.005
b_{031}	0.0081 ± 0.0002	0.0061 ± 0.0003	0.0098 ± 0.0005	0.0168 ± 0.0017
b_{202}	3.8004 ± 0.0003	3.8021 ± 0.0004	4.5567 ± 0.0006	4.291 ± 0.002
b_{112}	2.8003 ± 0.0005	2.7871 ± 0.0009	2.6705 ± 0.0011	2.524 ± 0.04
b_{022}	7.6032 ± 0.0006	7.6124 ± 0.0009	9.1181 ± 0.0012	8.599 ± 0.004
b_{103}	-0.0023 ± 0.0002	-0.0012 ± 0.0004	-0.0026 ± 0.0005	-0.0120 ± 0.0018
b_{013}	-0.00009 ± 0.00035	0.0002 ± 0.006	-0.0021 ± 0.0007	0.017 ± 0.003

[1] P. Langacker, Rev. Mod. Phys. **81**, 1199 (2009).
[2] A. Lionetto and A. Racioppi, ISRN High Energy Phys. **2012**, 903106 (2012).
[3] P. Anastasopoulos, F. Fucito, A. Lionetto, G. Pradisi, A. Racioppi, and Y. S. Stanev, Phys. Rev. D **78**, 085014 (2008).
[4] F. Fucito, A. Lionetto, A. Mammarella, and A. Racioppi, Eur. Phys. J. C **69**, 455 (2010).
[5] F. Fucito, A. Lionetto, and A. Mammarella, Phys. Rev. D **84**, 051702 (2011).
[6] E. Komatsu *et al.* (WMAP Collaboration), Astrophys. J. Suppl. Ser. **192**, 18 (2011).
[7] A. Lionetto and A. Racioppi, Nucl. Phys. **B831**, 329 (2010).
[8] F. Fucito, A. Lionetto, A. Racioppi, and D. Ricci Pacifici, Phys. Rev. D **82**, 115004 (2010).
[9] P. Langacker, R. W. Robinett, and J. L. Rosner, Phys. Rev. D **30**, 1470 (1984).
[10] Z.-q. Zhou, B. Xiao, Y.-k. Wang, and S.-h. Zhu, Phys. Rev. D **83**, 094022 (2011).
[11] F. Petriello and S. Quackenbush, Phys. Rev. D **77**, 115004 (2008).
[12] M. Cvetic and S. Godfrey, arXiv:hep-ph/9504216.
[13] M. Dittmar, A. S. Nicollerat, and A. Djouadi, Phys. Lett. B **583**, 111 (2004).
[14] S. Godfrey and T. A. W. Martin, Phys. Rev. Lett. **101**, 151803 (2008).
[15] Y.-k. Wang, B. Xiao, and S.-h. Zhu, Phys. Rev. D **83**, 015002 (2011).
[16] Y.-k. Wang, B. Xiao, and S.-h. Zhu, Phys. Rev. D **82**, 094011 (2010).
[17] P. Ferrario and G. Rodrigo, J. Phys. Conf. Ser. **171**, 012091 (2009).
[18] J. H. Kuhn and G. Rodrigo, Phys. Rev. Lett. **81**, 49 (1998).
[19] J. H. Kuhn and G. Rodrigo, Phys. Rev. D **59**, 054017 (1999).
[20] O. Antunano, J. H. Kuhn, and G. Rodrigo, Phys. Rev. D **77**, 014003 (2008).
[21] P. Ferrario and G. Rodrigo, Phys. Rev. D **78**, 094018 (2008).
[22] B. Xiao, Y. K. Wang, Z. Q. Zhou, and S. h. Zhu, Phys. Rev. D **83**, 057503 (2011).
[23] G. Corcella, I. G. Knowles, G. Marchesini, S. Moretti, K. Odagiri, P. Richardson, M. H. Seymour, and B. R. Webber, J. High Energy Phys. 01 (2001) 010.
[24] G. Corcella, I. G. Knowles, G. Marchesini, S. Moretti, K. Odagiri, P. Richardson, M. H. Seymour, and B. R. Webber, arXiv:hep-ph/0210213.
[25] G. Altarelli, B. Mele, and M. Ruiz-Altaba, Z. Phys. C **45**, 109 (1989); **47E**, 676 (1990).
[26] A. Mammarella, arXiv:1201.4340.
[27] G. Aad *et al.* (ATLAS Collaboration), J. High Energy Phys. 07 (2012) 019.
[28] G. Cattani, CERN Report No. CERN-THESIS-2011-247.
[29] F. Halzen and A. D. Martin (unpublished).